Research Square

Preprints are preliminary reports that have not undergone peer review.
They should not be considered conclusive, used to inform clinical practice,
or referenced by the media as validated information.

# Dynamical Scaling and Planetary Propagation of Tehuantepec Anticyclonic Eddies

**Federico Angel Velázquez-Muñoz**

federico.velazquez@academicos.udg.mx

Universidad de Guadalajara

**Ever Gustavo Velázquez-Galván**

**Raúl Candelario Cruz-Gómez**

Universidad de Guadalajara

**Cesar Monzon**

Universidad de Guadalajara

**Research Article**

**Keywords:**

**Posted Date:** November 13th, 2026

**DOI:** https://doi.org/10.21203/rs.3.rs-11156332/v1

**License:** This work is licensed under a Creative Commons Attribution 4.0 International License.
Read Full License

**Additional Declarations:** No competing interests reported.

# Dynamical Scaling and Planetary Propagation of Tehuantepec Anticyclonic Eddies

Federico Angel Velázquez-Muñoz[1*],
Eber Gustavo Velázquez-Galván, Raúl Candelario Cruz-Gómez[1],
César Monzón[3]

[1*]Departamento de Física, Centro Universitario de Ciencias Exactas e Ingenierías (CUCEI), Universidad de Guadalajara, Av. Revolución 1500, Guadalajara, 44430, Jalisco, Mexico.
[2]Departamento de Ingeniería de Proyectos, Centro Universitario de Ciencias Exactas e Ingenierías (CUCEI), Universidad de Guadalajara, Av. José Parres Arias 150, Zapopan, 45100, Jalisco, Mexico.

*Corresponding author(s). E-mail(s):
federico.velazquez@academicos.udg.mx;
Contributing authors: eber.velazquez@example.com;
raul.cruz@academicos.udg.mx; cesar.monzon@academicos.udg.mx;

**Abstract**

The Northeastern Tropical Pacific (NETP) is strongly influenced by Tehuantepec gap-wind jets, which spin up energetic mesoscale eddies. In this study, we combine multi-mission altimetry products, Cross-Calibrated Multi-Platform (CCMP) surface wind-stress data, and three-dimensional numerical simulations Princeton Ocean Model (POM) to investigate the evolution and dynamical scaling of Tehuantepec anticyclonic eddies. Automated vector-geometry tracking via the Angular Momentum Eddy Detection and Tracking Algorithm (AMEDA) identified 44 long-lived anticyclonic eddies between 2007 and 2023, yielding an average generation rate of 2.75 eddies per season. The tracked eddies exhibit mean translation speeds of 11.67 km/day, with propagation distances up to 3,333 km. The advective nonlinearity parameter $\boldsymbol{\alpha = U_\theta / U_c}$, where $\boldsymbol{U_\theta}$ is the maximum azimuthal velocity and $\boldsymbol{U_c}$ is the eddy translation speed, ranges from 3.2 to 4.7, indicating highly nonlinear and coherent structures. Numerical experiments show that single short-duration wind pulses generate weak eddies, whereas realistic multi-event forcing produces cumulative, stepwise spin-up. Sensitivity experiments further show that upper-layer thickness strongly controls

eddy intensity ($\boldsymbol{U_\theta \propto H^{-1}}$), while the vortex radius remains nearly unchanged ($\boldsymbol{R \approx 81}$–$\boldsymbol{84}$ km). Westward translation is also consistent, to first order, with the planetary scaling $\boldsymbol{U_c \sim \beta R^2}$. These results link wind impulse, upper-ocean stratification, vortex intensity, and planetary propagation within a common dynamical framework.

**Keywords:** Mesoscale eddies, Tehuantepec wind jets, AMEDA detection, Princeton Ocean Model, Advective nonlinearity, Upper-ocean stratification

# 1 Introduction

The atmospheric and oceanic dynamics of the Northeastern Tropical Pacific (NETP) are heavily influenced by the unique topography of Central America [1]. During the boreal winter, high-pressure systems originating over North America migrate southward, establishing a strong pressure gradient across the Isthmus of Tehuantepec [2]. This gradient forces cold, dense air to accelerate through Chivela Pass, a narrow, low-elevation gap in the Sierra Madre mountain range [3]. Upon exiting the pass, these winds emerge over the Gulf of Tehuantepec (GT) as intense, offshore gap-wind jets, locally known as Tehuanos or Nortes, which routinely reach speeds of 10 to 24 m/s and can occasionally exceed 50 m/s [4, 5]. Rather than remaining confined to a narrow corridor, these high-speed winds fan out across the gulf and veer anticyclonically to the right under the influence of the Coriolis force, creating a highly asymmetrical fanlike wind pattern [3].

These intense offshore wind jets exert strong wind stress on the ocean surface, driving a vigorous localized oceanic response [5]. Driven by Ekman dynamics, the wind-stress curl changes sign across the jet axis, with negative values to the west and positive values to the east. This dipolar structure promotes anticyclonic circulation to the west and cyclonic circulation to the east [5–7]. However, the resulting dipolar circulation exhibits a marked structural asymmetry [8]. Cyclonic eddies elevate the thermocline and are generally shallow and short-lived; intense vertical mixing and boundary friction drive their rapid decay, keeping them confined near the coast [7]. Conversely, anticyclonic eddies are remarkably robust, deep-reaching, and persistent [6, 9]. They depress the thermocline and can endure in the open ocean for several months, propagating westward or southwestward over distances ranging from 1,500 to more than 4,500 km across the Pacific Ocean [10–12].

An essential aspect of these long-lived eddies do not always arise from a single, isolated atmospheric forcing event. Instead, the upper ocean integrates high-frequency atmospheric variability, as successive gap-wind pulses repeatedly inject kinetic energy into a developing vortex. This process acts via a "whip and top" mechanism that progressively reinforces the circulation before the eddy migrates offshore [13]. Furthermore, to preserve their structural properties and persist for several months while propagating through sheared background currents, these mesoscale eddies must behave as highly nonlinear, coherent structures [12, 14]. Advective nonlinearity is typically quantified by the parameter $\alpha = U_\theta/U_c$, where $U_\theta$ is the maximum azimuthal velocity

and $U_c$ is the eddy translation speed. Values of $\alpha > 1$ indicate that internal rotation dominates over translation, promoting fluid entrapment and coherent transport. Consequently, such nonlinear eddies effectively retain water within their cores over vast distances, transporting heat, salt, and biogeochemical properties across the ocean.

To characterize these structures and examine their evolution, we apply the Angular Momentum Eddy Detection and Tracking Algorithm (AMEDA) to gridded altimetric velocity fields. The resulting trajectories provide the eddy radius, azimuthal velocity, relative vorticity, translation speed, and advective nonlinearity throughout their lifetimes. We then use the Princeton Ocean Model (POM) to reproduce the observed eddy evolution under idealized and realistic atmospheric forcing. The numerical experiments are used to examine the effects of recurrent wind forcing and upper–ocean stratification on vortex intensification and westward propagation. In particular, we investigate how recurrent wind forcing and upper-layer thickness regulate eddy intensity and whether the subsequent translation can be interpreted in terms of planetary $\beta$-drift scaling.

## 2 Data sets and methods

This section describes the observational datasets, the eddy detection and tracking procedure, and the numerical model configuration. The study domain (Fig. 1) covers a region of the NETP spanning from 120°W to 90°W and 5°N to 20°N. The Gulf of Tehuantepec lies in the northeastern sector of the domain, where strong and intermittent gap-wind jets drive intense ocean–atmosphere interactions. These winds promote local upwelling and mesoscale eddy generation.

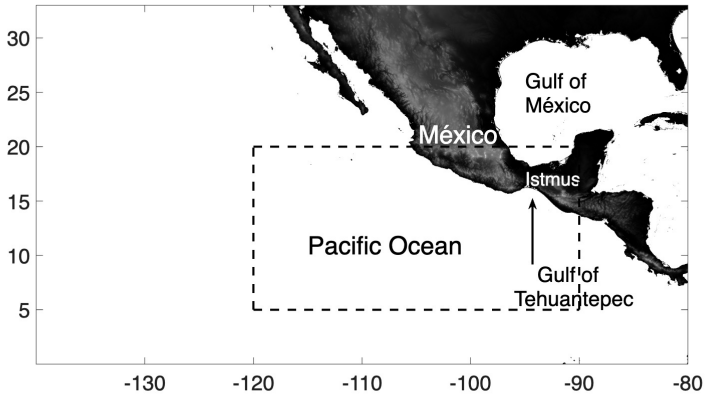



**Fig. 1** Study domain in the Northeastern Tropical Pacific (NETP). The dashed rectangle indicates the analyzed region, and the Gulf of Tehuantepec (GT) is located along the southeastern coast of Mexico.

## 2.1 AVISO altimetry data

We use Level-4 (L4) multi-mission gridded altimetry products generated by the CNES/CLS Data Unification and Altimeter Combination System (DUACS) and distributed through the AVISO/Copernicus Marine Service. The product combines along-track altimeter observations from multiple satellite missions and maps them onto a regular grid using the Multiscale Inversion of Ocean Surface Topography (MIOST) algorithm. Daily fields are provided at a spatial resolution of $0.125° \times 0.125°$.

The variables used in this study include sea level anomaly (SLA), absolute dynamic topography (ADT), and geostrophic velocity fields. The latter comprise zonal and meridional velocity anomalies ($u_{gosa}$, $v_{gosa}$) and absolute geostrophic velocities ($u_{gos}$, $v_{gos}$).

The temporal variance of SLA reveals a band of enhanced mesoscale variability extending westward from the Gulf of Tehuantepec, approximately between 100°W and 111°W and centered near 11°N, as shown in Fig. 2a.

## 2.2 CCMP wind stress data

Surface wind forcing is characterized using the Cross-Calibrated Multi-Platform (CCMP) Version 3.1 product [15, 16]. CCMP provides spatially complete Level-4 wind fields at 6-hour intervals on a global $0.25° \times 0.25°$ grid [16]. The product combines multi-platform satellite observations with numerical weather prediction fields through a Variational Analysis Method (VAM).

We use the zonal and meridional wind stress components, $\tau_x$ and $\tau_y$, to characterize the temporal variability and spatial extent of Tehuano wind forcing. The region directly influenced by the gap-wind jet was identified from the cross-correlation between the node of maximum temporal variance and neighboring grid nodes; the red dot in Fig. 2a. The corresponding time series of $\tau_x$ and $\tau_y$ at the reference location are shown in Fig. 2b, illustrating the strong seasonal and intermittent nature of the forcing.

## 2.3 Eddy detection and tracking

AMEDA was applied to two-dimensional velocity fields to identify and track mesoscale coherent vortices [17]. The method combines dynamical and geometrical properties of the flow to characterize their structure and evolution. The algorithm computes kinetic energy, relative vorticity, Okubo–Weiss (OW), local Okubo–Weiss (LOW), and local normalized angular momentum (LNAM) fields. Candidate eddy centers are identified from local extrema of LNAM satisfying $|LNAM| \geq 0.7$. Only regions with LOW $< 0$, where rotation dominates over deformation, are retained. A center is subsequently validated when it is enclosed by at least two closed streamlines of SSH or stream function.

For each validated vortex, AMEDA determines the characteristic radius $R_{max}$ from the closed streamline where the mean azimuthal velocity reaches its maximum value $U_\theta$. The algorithm then links eddy centers between successive time steps using a global cost function $\epsilon_{ji}$. This function accounts for changes in position, radius, intensity, and temporal separation. The optimal assignment is obtained with the Kuhn–Munkres

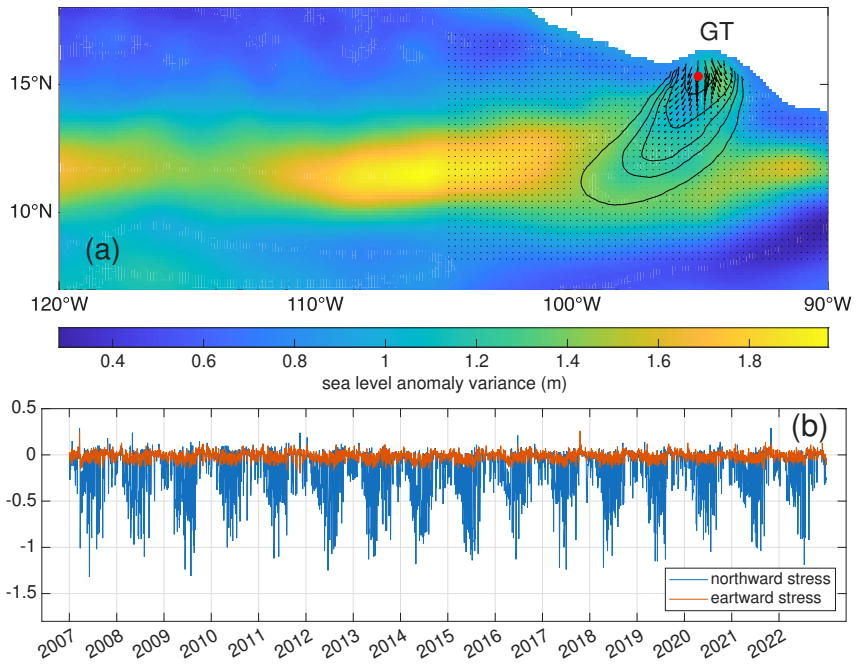



**Fig. 2** (a) Temporal variance of sea level anomaly (SLA) in the NETP. The red dot indicates the coastal reference location in the Gulf of Tehuantepec, while the contours delineate the region influenced by Tehuano wind events. (b) Surface wind stress components $(\tau_x, \tau_y)$ at the reference location.

algorithm, producing unique eddy trajectories and allowing merging and splitting events to be identified.

For each trajectory, we retain the eddy-center coordinates $(x_1, y_1)$, characteristic radius $R_{max}$, maximum azimuthal velocity $U_\theta$, and relative vorticity $\zeta_1$. These quantities are used to characterize the temporal evolution and dynamical properties of the detected eddies.

## 2.4 Numerical model setup

POM was used to investigate the generation, structural evolution, and sensitivity of Tehuantepec anticyclonic eddies to upper-ocean stratification [18]. The numerical domain coincides with the regional domain shown in Fig. 1. Bottom bathymetry was derived from the GEBCO 2024 grid [19] and interpolated onto the model grid. The horizontal resolution is approximately 5.5 km, with 41 terrain-following sigma levels in the vertical. The model was initialized from rest with uniform surface elevation.

The spatial structure of the atmospheric forcing was derived from a composite of CCMP wind events over 16 seasons (2007–2022). Strong northerly gap-wind events were identified when the meridional wind stress satisfied $\tau_y < -0.5$ N/m$^2$. The wind-jet footprint was defined by $|\boldsymbol{\tau}| \geq 0.1$ N/m$^2$, with values outside this region set to zero. The resulting pattern was normalized by the maximum meridional wind-stress magnitude to obtain the spatial forcing template shown in Fig. 3a.

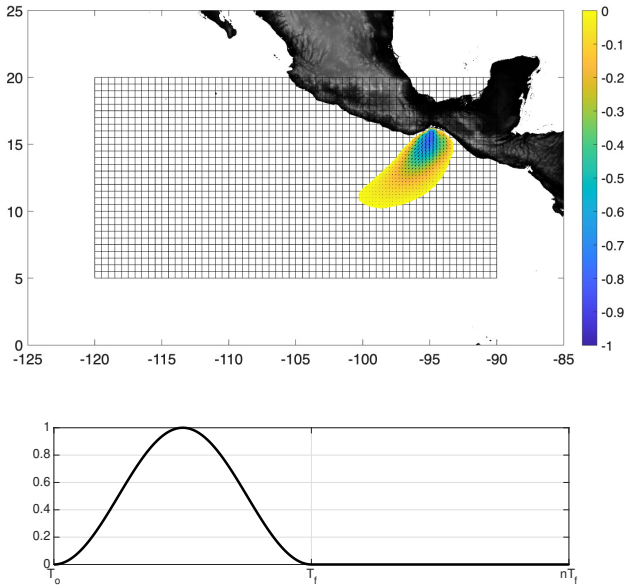



**Fig. 3** (a) Normalized spatial wind-stress template derived from composite CCMP northerly wind events over the Gulf of Tehuantepec. (b) Temporal modulation function $T(t)$ used to generate isolated wind events lasting 2, 4, 6, and 8 days.

Two temporal forcing configurations were considered. For the idealized experiments, the wind stress was modulated using

$$T(t) = \frac{1}{2}\left[1 - \cos\left(\frac{2\pi t}{t_w}\right)\right], \qquad t \leq t_w,$$

where $t_w$ is the duration of the wind event [20]. Values of $t_w = 2$, 4, 6, and 8 days were examined, as shown in Fig. 3b.

A second experiment reproduced the recurrent nature of the observed forcing. The temporal modulation was prescribed from the continuous $\tau_y$ record between October 1, 2013, and February 28, 2014, thereby retaining the sequence of gap-wind pulses observed during the season.

The initial temperature, salinity, and density fields were horizontally homogeneous, preventing the development of initial geostrophic shear. To examine the influence of upper-ocean stratification, two configurations were considered, with the principal thermocline/pycnocline centered at $H = 50$ m and $H = 100$ m, as shown in Fig. 4.

# 3 Results

## 3.1 Observational tracking and kinematic properties

AMEDA identified 44 long-lived anticyclonic eddies over the 16 gap-wind seasons analyzed between 2007 and 2023, corresponding to an average generation rate of 2.75

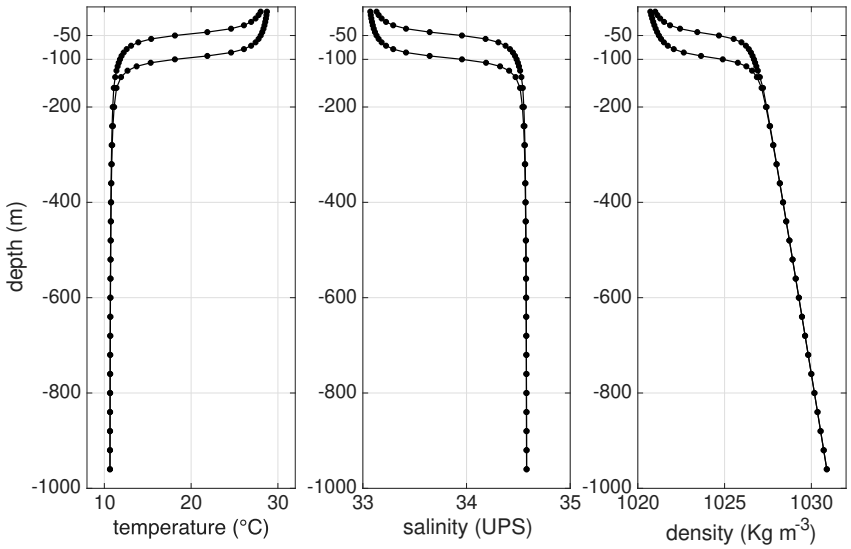



**Fig. 4** Initial vertical profiles of (a) temperature, (b) salinity, and (c) density used in the POM sensitivity experiments. Dashed and solid curves correspond to thermocline/pycnocline depths of 50 and 100 m, respectively.

eddies per season, as shown in Fig. 5. This value is lower than previous altimetric estimates [11] and may partly reflect the stricter spatiotemporal coherence criteria imposed by AMEDA.

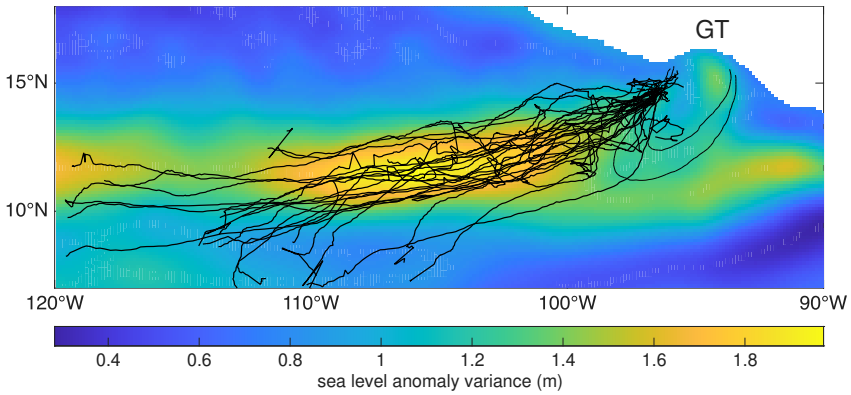



**Fig. 5** Trajectories of long-lived anticyclonic eddies identified by AMEDA in the Gulf of Tehuantepec over 16 gap-wind seasons (2007–2023).

The main kinematic and dynamical properties of the tracked eddies are summarized in Table 1.

A representative example of three anticyclonic eddies during the 2013–2014 season is shown in Fig. 6.

**Table 1** Kinematic and dynamical properties of AMEDA-tracked anticyclonic eddies in the NETP during 2007–2023.

| Parameter | Mean | Min | Max | Std. Dev. |
|---|---|---|---|---|
| Lifespan (days) | 142.5 | 35 | 283 | 58.2 |
| Propagation Distance (km) | 2,152 | 412 | 3,333 | 724 |
| Translation Speed $U_c$ (km/day) | 11.67 | 6.94 | 18.72 | 2.45 |
| Characteristic Radius $R_{max}$ (km) | 116.3 | 62.1 | 168.4 | 18.6 |
| Azimuthal Velocity $U_\theta$ (m/s) | 0.439 | 0.017 | 0.932 | 0.142 |
| Relative Vorticity $\zeta$ ($10^{-5}$ s$^{-1}$) | $-0.805$ | $-2.140$ | $-0.110$ | 0.380 |
| Nonlinearity Parameter $\alpha = U_\theta/U_c$ | 3.85 | 3.20 | 4.70 | 0.42 |

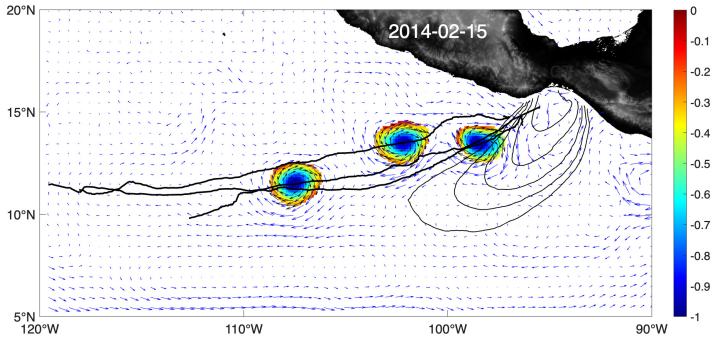



**Fig. 6** Geostrophic velocity anomaly field and trajectories of three anticyclonic eddies during the 2013–2014 season. Black vectors indicate the high-speed eddy cores, while the colored trajectories represent the evolution of relative vorticity.

The velocity field reveals compact regions of enhanced orbital motion associated with each tracked vortex. Along these trajectories, we extract time series of the maximum azimuthal velocity $U_\theta$ and relative vorticity $\zeta$. Figure 7 illustrates the temporal evolution of these kinematic properties for the three eddies alongside the meridional wind stress $\tau_y$.

During the vortex intensification phase, $U_\theta$ increases while the magnitude of the anticyclonic relative vorticity $|\zeta|$ strengthens. However, the spin-up timescale varies among the three vortices: the first two require nearly two months to reach peak intensity, whereas the third attains its maximum azimuthal velocity within approximately one month. Notably, peak $U_\theta$ lags the maximum relative-vorticity magnitude by roughly 14 days, revealing a distinct phase lag between the evolution of core vorticity and orbital speed.

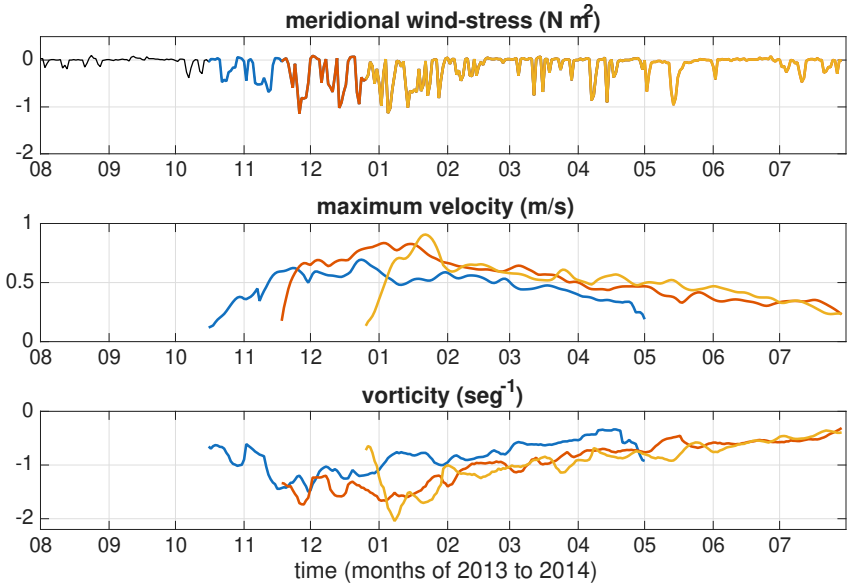



**Fig. 7** Temporal evolution during the 2013–2014 season of (a) meridional wind stress $\tau_y$ over the Gulf of Tehuantepec, (b) maximum azimuthal velocity $U_\theta$, and (c) core relative vorticity $\zeta$ for three consecutive anticyclonic eddies.

The advective nonlinearity parameter $\alpha = U_\theta/U_c$ ranges from 3.2 to 4.7 for the tracked eddies. Values well above unity indicate that orbital velocities dominate over eddy translation, consistent with strongly nonlinear vortices and conditions favorable for coherent fluid transport.

## 3.2 Numerical experiments

Single-event experiments show that isolated wind pulses can generate anticyclonic vortices, but their intensity and propagation differ substantially from the observed eddies. The 4-, 6-, and 8-day experiments produce coherent westward-propagating structures, as shown in Fig. 8.

The 2-day pulse does not provide sufficient forcing to produce a persistent vortex. For the longer isolated events, however, coherent vortices are generated, although their translation speeds, evaluated over the 90-day integrations after excluding the initial 30-day spin-up period, remain approximately 50% lower than the altimetric values. Peak relative-vorticity magnitudes are also 20%–40% weaker, as summarized in Table 2.

A different response emerges when the model is forced with the recurrent 2013–2014 wind sequence shown in Fig. 9a. In this case, the model generates three principal anticyclonic eddies whose westward trajectories resemble those identified from altimetry, as shown by comparison of Figs. 9b,c with Fig. 6. The observed and simulated eddy properties are compared in Table 2.

The modeled eddy radii remain between approximately 81 and 84 km, smaller than the mean altimetric radius of about 116 km. This difference may partly reflect the

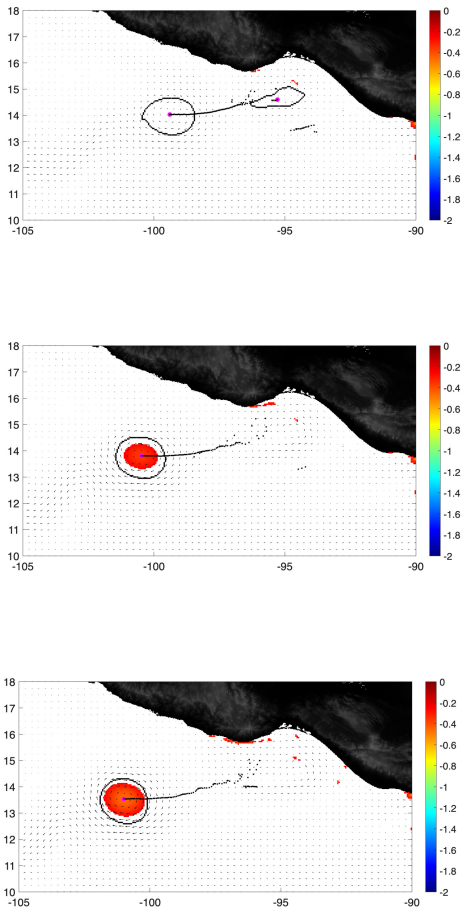



**Fig. 8** Simulated eddy trajectories and sea surface elevation under isolated wind forcing lasting (a) 4, (b) 6, and (c) 8 days.

**Table 2** Comparison of physical parameters between satellite observations and POM numerical experiments (2013–2014 season).

| Dataset / Experiment | $R_{max}$ (km) | $U_\theta^{max}$ (m/s) | $\zeta_{max}$ ($10^{-5}$ s$^{-1}$) | $U_c$ (km/day) | $\alpha = U_\theta / U_c$ |
|---|---|---|---|---|---|
| AVISO Altimetry | $116.3 \pm 18$ | 0.84 | $-2.14$ | 9.8 | 3.85 |
| Single Event (6-day) | $78.2 \pm 12$ | 0.38 | $-0.95$ | 5.2 | 2.10 |
| Realistic ($H = 50$ m) | $81.4 \pm 10$ | 1.58 | $-2.68$ | 10.4 | 7.32 |
| Realistic ($H = 100$ m) | $84.1 \pm 11$ | 0.86 | $-1.58$ | 10.4 | 4.84 |

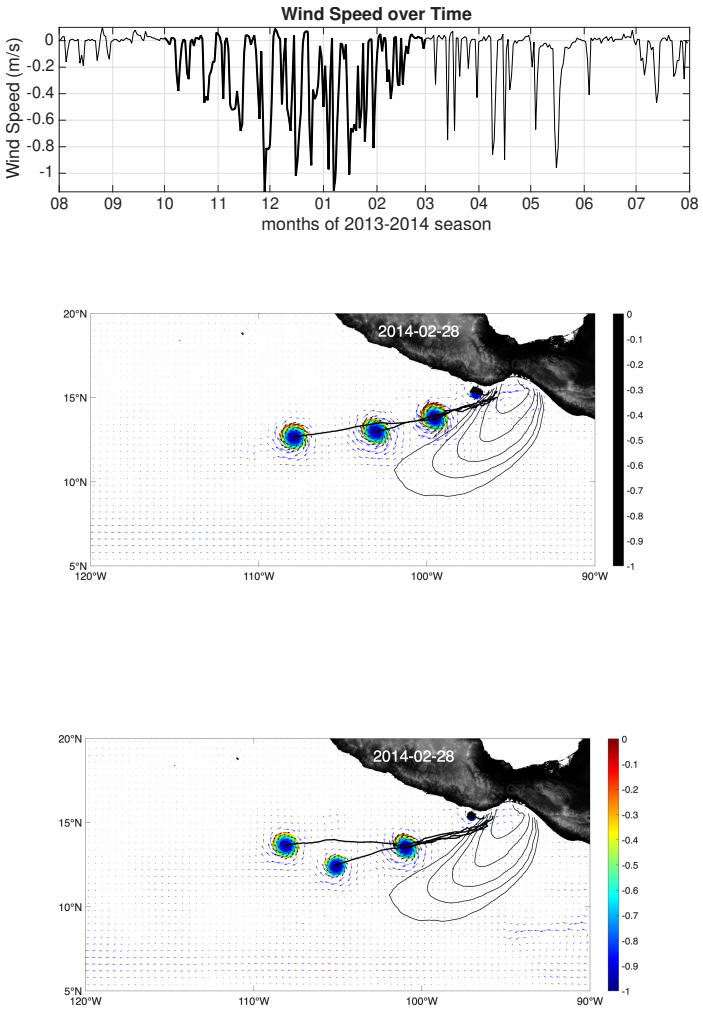



**Fig. 9** Numerical experiment forced by the observed 2013–2014 wind-stress sequence. (a) Meridional wind stress $\tau_y$ used as forcing. Eddy trajectories obtained for thermocline depths of (b) $H = 50$ m and (c) $H = 100$ m.

spatial smoothing inherent in gridded altimetry products, which can broaden velocity structures and their diagnosed boundaries.

Despite this difference in horizontal scale, the strongest sensitivity to upper-layer thickness appears in the orbital velocity. For $H = 50$ m, the simulated peak azimuthal velocity reaches $U_\theta = 1.58$ m/s, exceeding the observed value. When the thermocline is deepened to $H = 100$ m, the peak velocity decreases to $U_\theta = 0.86$ m/s, closely approaching the observed value of 0.84 m/s.

# 4 Physical Mechanisms and Dynamical Interpretation

The numerical experiments indicate that two processes are central to the evolution of Tehuantepec anticyclonic eddies. Wind forcing controls the initial spin-up, while upper-ocean structure regulates the resulting vortex intensity. After the eddy leaves the forcing region, baroclinic adjustment and planetary rotation become increasingly important for its structure and westward propagation.

## 4.1 Stratification control and momentum scaling

The strong sensitivity of $U_\theta$ to upper-layer thickness can be interpreted from a simple momentum balance. During wind-driven spin-up, the characteristic horizontal velocity satisfies

$$\frac{\partial U}{\partial t} \sim \frac{\tau(t)}{\rho_0 H}, \tag{1}$$

where $H$ is the upper-layer thickness and $\rho_0$ is the reference density. Thus, the same surface stress produces a larger acceleration when the forced layer is shallower.

Integrating Eq. (1) over a wind event of duration $T_{\text{event}}$ gives

$$\Delta U \sim \frac{1}{\rho_0 H} \int_0^{T_{\text{event}}} \tau(t)\, dt = \frac{I_\tau}{\rho_0 H}, \tag{2}$$

where $I_\tau$ represents the wind-stress impulse. Equation (2) therefore shows that, for comparable wind forcing, the velocity response varies inversely with $H$.

If a comparable fraction of this momentum is converted into vortex rotation in both experiments, the azimuthal velocity should follow

$$U_\theta \propto \frac{I_\tau}{\rho_0 H}.$$

For identical atmospheric forcing, this predicts

$$\frac{U_{\theta,50}}{U_{\theta,100}} \sim \frac{H_{100}}{H_{50}} = 2.0. \tag{3}$$

The numerical experiments closely follow this scaling. The simulated peak velocities are 1.58 and 0.86 m/s for $H = 50$ and 100 m, respectively, giving $U_{\theta,50}/U_{\theta,100} = 1.84$, only about 8% below the inverse-depth prediction.

The same dependence is evident in the mean azimuthal velocity, which decreases from 1.08 to 0.62 m/s as $H$ increases from 50 to 100 m. In contrast, the mean vortex radius changes only slightly, from 81.4 to 84.1 km. The upper-layer thickness therefore exerts a strong control on vortex intensity while having comparatively little influence on its horizontal scale.

## 4.2 Baroclinic adjustment and horizontal scale

The numerical experiments show that upper-layer thickness strongly affects vortex intensity, while the horizontal radius remains comparatively insensitive to $H$. This

behavior can be examined in terms of the baroclinic deformation scale. For a reduced-gravity system, the Rossby deformation radius is

$$R_d = \frac{\sqrt{g'H}}{f}, \qquad g' = g\frac{\Delta\rho}{\rho_0}, \tag{4}$$

where $g'$ is the reduced gravity and $f$ is the Coriolis parameter.

Using $\Delta\rho \approx 6.0$ kg/m$^3$ ($g' \approx 0.058$ m/s$^2$) and $f \approx 3.8 \times 10^{-5}$ s$^{-1}$ at 15°N gives $R_{d,50} \approx 45$ km and $R_{d,100} \approx 64$ km.

The relation between the deformation scale and the vortex radius can be expressed through the Burger number

$$Bu = \left(\frac{R_d}{R}\right)^2.$$

The two experiments yield $Bu_{50} \approx 0.35$ and $Bu_{100} \approx 0.68$. Deepening the upper layer therefore moves the vortex closer to a regime with $Bu = \mathcal{O}(1)$, where the deformation radius and the horizontal vortex scale become comparable.

This result complements the momentum scaling derived above. Increasing $H$ substantially reduces $U_\theta$, while the vortex radius changes only slightly. At the same time, the increase in $R_d$ raises the Burger number toward unity. Upper-layer thickness therefore strongly controls vortex intensity while simultaneously modulating the energetic balance between the deformation scale and horizontal vortex geometry.

## 4.3 Kinematic scaling and planetary translation

The internal kinematics of the simulated vortices also follow a simple scaling. Core relative-vorticity magnitude is strongly correlated with $U_\theta/R$ in both experiments ($r > 0.99$), giving

$$|\zeta| \approx 2.0\,\frac{U_\theta}{R}.$$

Thus, the decrease in vortex intensity with increasing $H$ is accompanied by a corresponding reduction in core vorticity, while the radius remains nearly unchanged.

The westward translation can be compared with the planetary $\beta$-drift velocity scale

$$c_\beta \sim \beta R^2.$$

Using the simulated vortex radii gives characteristic drift speeds of 13.0–13.9 km/day. These values are close to the trajectory-derived speeds of approximately 10.4 km/day, indicating that $\beta R^2$ provides a first-order scale for the westward propagation.

Combining the wind-impulse scaling $U_\theta \sim I_\tau/(\rho_0 H)$ with the planetary translation scale leads to

$$\alpha_\beta \equiv \frac{U_\theta}{\beta R^2} \sim \frac{I_\tau}{\rho_0 H \beta R^2}. \tag{5}$$

The parameter $\alpha_\beta$ compares the velocity generated by atmospheric spin-up with the characteristic velocity associated with planetary propagation. It therefore provides a compact measure of the competition between wind-driven vortex intensification and $\beta$-controlled translation.

The principal dimensional and nondimensional diagnostics for the two upper-layer configurations are summarized in Table 3.

**Table 3** Dimensional and nondimensional dynamical diagnostics for the two upper-layer configurations.

| Parameter / Diagnostic | $H = 50$ m | $H = 100$ m |
|---|---|---|
| Mean Azimuthal Speed $\langle U_\theta \rangle$ (m/s) | 1.084 | 0.624 |
| Peak Azimuthal Speed $U_\theta^{max}$ (m/s) | 1.576 | 0.858 |
| Mean Radius $\langle R \rangle$ (km) | 81.4 | 84.1 |
| Mean Relative Vorticity $\langle \lvert\zeta\rvert \rangle$ ($10^{-5}$ s$^{-1}$) | 2.685 | 1.581 |
| Burger Number $Bu = (R_d/R)^2$ | 0.348 | 0.675 |
| Planetary Velocity Scale $\beta R^2$ (km/day) | 13.03 | 13.94 |
| Trajectory Drift Speed $U_c$ (km/day) | 10.36 | 10.35 |
| Nonlinearity Ratio $\alpha_\beta = U_\theta/(\beta R^2)$ | 7.32 | 4.84 |

Table 3 reveals a clear separation between vortex intensity and horizontal scale. Increasing the upper-layer thickness from 50 to 100 m reduces both the mean azimuthal velocity and the relative-vorticity magnitude by approximately 40%–45%, while the mean radius changes by only about 3%.

In contrast, the Burger number increases from 0.35 to 0.68 as the deformation radius grows with $H$. The deeper configuration therefore approaches a regime in which the deformation radius and vortex radius are of comparable magnitude. Despite these structural changes, the planetary velocity scale $\beta R^2$ and the trajectory-derived drift speed $U_c$ remain nearly unchanged. This indicates that upper-layer thickness primarily controls the internal vortex intensity, whereas westward propagation is governed mainly by the horizontal vortex scale and planetary vorticity gradient.

# 5 Discussion

The identification of 44 long-lived anticyclones over 16 gap-wind seasons yields an average generation rate of 2.75 eddies per season, lower than the 3.5 Tehuantepec eddies per year reported by Palacios and Bograd [11]. Part of this difference may arise from the detection methodology. Fixed SLA thresholds and derivative-based Okubo–Weiss criteria can retain transient or noisy structures [7, 12], whereas AMEDA combines velocity-field geometry, kinematic criteria, and temporal tracking [17]. The resulting census therefore provides a more restrictive estimate of long-lived coherent anticyclones.

Within this observational framework, the numerical experiments show that eddy development depends strongly on the temporal history of the forcing. Isolated wind pulses generate relatively weak vortices, whereas recurrent Tehuano events produce cumulative spin-up, consistent with the successive reinforcement proposed by Chang et al. [13]. Consequently, the oceanic response reflects the accumulated wind-stress impulse rather than the duration of a single event alone.

This dependence on forcing history is complemented by a strong sensitivity to upper-layer thickness. Doubling $H$ from 50 to 100 m reduces the peak azimuthal velocity from 1.58 to 0.86 m/s, while the vortex radius changes only weakly. This response is consistent with $U_\theta \propto I_\tau/(\rho_0 H)$, for which the predicted velocity ratio of 2.0 is close to the simulated value of 1.84. Thus, the atmospheric impulse and the thickness of the forced layer act together to determine vortex intensity.

At the same time, the horizontal structure and westward propagation show a much weaker sensitivity to $H$. As the upper layer deepens, the Burger number increases from 0.35 to 0.68 because the deformation radius grows while the vortex radius remains nearly unchanged. The deeper configuration therefore moves closer to a regime with $Bu = \mathcal{O}(1)$. Consistently, the trajectory speed remains close to 10.4 km/day in both experiments, while the planetary velocity scale $\beta R^2$ varies only from approximately 13.0 to 13.9 km/day. This contrast suggests that upper-layer thickness primarily regulates vortex intensity, whereas westward propagation is more closely linked to the horizontal vortex scale and the planetary vorticity gradient.

Consistent with this separation between internal intensity and translation, the observed advective nonlinearity parameter $\alpha = U_\theta/U_c$ remains well above unity, ranging from 3.2 to 4.7. Orbital motion therefore dominates over translation, indicating strongly nonlinear vortices and conditions favorable for fluid trapping [14]. This nonlinear character helps explain the ability of Tehuantepec anticyclones to transport heat, salt, and biogeochemical properties over long distances across the Northeastern Tropical Pacific.

# 6 Conclusion

This study combines satellite observations and numerical experiments to examine the formation, evolution, and propagation of long-lived anticyclonic eddies generated by Tehuantepec gap winds. AMEDA tracking identifies 44 coherent anticyclones over 16 gap-wind seasons, corresponding to an average generation rate of 2.75 eddies per season.

Within this observational framework, the numerical experiments show that vortex development depends strongly on the temporal structure of the atmospheric forcing. Isolated wind pulses generate relatively weak vortices, whereas recurrent Tehuano events produce cumulative spin-up through successive momentum input. The resulting response is therefore better described by the accumulated wind-stress impulse than by the duration of an individual event.

In addition to forcing history, upper-layer thickness provides a strong control on vortex intensity. For comparable forcing, the azimuthal velocity follows the scaling $U_\theta \propto H^{-1}$, while the vortex radius remains comparatively insensitive to $H$. At the same time, the Burger number increases from 0.35 to 0.68 as the deformation radius grows, bringing the deeper configuration closer to a regime in which the deformation radius and vortex radius are comparable.

In contrast to the strong response of vortex intensity, westward translation changes little between the two upper-layer configurations and is consistent, to first order, with the planetary velocity scale $\beta R^2$. This separation suggests that upper-ocean structure

primarily regulates the internal circulation, whereas horizontal vortex scale and the planetary vorticity gradient exert stronger control on propagation.

Finally, the observed values of $\alpha = U_\theta/U_c > 1$ indicate strongly nonlinear eddies whose orbital motion dominates over translation. Such conditions favor coherent fluid transport over long distances across the Northeastern Tropical Pacific.

**Supplementary information.** Not applicable.

**Acknowledgements.** The authors acknowledge CNES/CLS DUACS and Copernicus Marine Service for providing altimetry products, and Remote Sensing Systems for CCMP wind fields. Numerical simulations were performed using the Princeton Ocean Model (POM).

The authors express their sincere gratitude to the Universidad de Guadalajara (UdeG) and the Centro Universitario de Ciencias Exactas e Ingenierías (CUCEI) for their continuous support, institutional resources, and academic infrastructure provided throughout the development of this research project and the preparation of this manuscript.

# Declarations

- **Funding:** This research received no specific grant from funding agencies in the public, commercial, or not-for-profit sectors.
- **Conflict of interest/Competing interests:** The authors declare that they have no competing interests.
- **Ethics approval and consent to participate:** Not applicable.
- **Consent for publication:** Not applicable.
- **Data availability:** Altimetry data are available via Copernicus Marine Service (CMEMS). CCMP wind data are available from Remote Sensing Systems (www.remss.com). Bathymetry data are available from GEBCO 2024.
- **Materials availability:** Not applicable.
- **Code availability:** AMEDA software is available at GitHub (https://github.com/1373/AMEDA). Princeton Ocean Model code is available from the POM user group.
- **Author contribution:** All authors contributed equally to manuscript preparation, data analysis, and numerical modeling.

# Appendix A Methodological Supplement: AMEDA Tracking Parameters

The AMEDA algorithm was configured with a normalized angular momentum threshold of $|LNAM| \geq 0.7$, a local window size $L_b = 3$ grid cells, and an eddy core boundary criterion where azimuthal speed reaches maximum velocity ($U_{max}$). Velocity decay at the outer edge was constrained to $U_{end} \geq 0.97U_{max}$. Trajectory linkage permitted a dynamic search radius based on propagation limit $U_c = 6.5$ km/day with a temporal correlation gap tolerance $T_c = 4$ days.

# References


[1] Kessler, W.S.: The circulation of the eastern tropical Pacific: A review. Progress in Oceanography **69**(2–4), 181–217 (2006)

[2] Romero-Centeno, R., Zavala-Hidalgo, J., Gallegos, A., O'Brien, J.J.: Isthmus of Tehuantepec wind climatology and ENSO signal. Journal of Climate **16**(15), 2628–2639 (2003)

[3] Steenburgh, W.J., Schultz, D.M., Colle, B.A.: The structure and evolution of gap outflow over the Gulf of Tehuantepec, Mexico. Monthly Weather Review **126**(10), 2673–2691 (1998)

[4] Clarke, A.J.: Inertial wind path and sea surface temperature patterns near the Gulf of Tehuantepec and Gulf of Papagayo. Journal of Geophysical Research: Oceans **93**(C12), 15491–15501 (1988)

[5] Barton, E.D., Argote, M.L., Brown, J., Kosro, P.M., Lavín, M.F., Robles, J.M., Smith, R.L., Trasviña, A., Vélez, H.S.: Supersquirt: Dynamics of the Gulf of Tehuantepec, Mexico. Oceanography **6**(1), 23–30 (1993)

[6] Trasviña, A., Barton, E.D., Brown, J., Vélez, H.S., Kosro, P.M., Smith, R.L.: Offshore wind forcing in the Gulf of Tehuantepec, Mexico: The asymmetric circulation. Journal of Geophysical Research: Oceans **100**(C10), 20649–20663 (1995)

[7] Santiago-García, M.W., Parés-Sierra, A.F., Trasviña, A.: Dipole-wind interactions under gap wind jet conditions in the Gulf of Tehuantepec, Mexico: A surface drifter and satellite database analysis. PLoS ONE **14**(12), 0226366 (2019)

[8] Trasviña, A., Barton, E.D.: Summer circulation in the Mexican tropical Pacific. Deep-Sea Research Part I: Oceanographic Research Papers **55**(5), 587–607 (2008)

[9] Liang, J.-H., McWilliams, J.C., Kurian, J., Colas, F., Wang, P., Uchiyama, Y.: Mesoscale variability in the northeastern tropical Pacific: Forcing mechanisms and eddy properties. Journal of Geophysical Research: Oceans **117**(C7), 07003 (2012)

[10] Müller-Karger, F.E., Fuentes-Yaco, C.: Characteristics of wind-generated rings in the eastern tropical Pacific Ocean. Journal of Geophysical Research: Oceans **105**(C1), 1271–1284 (2000)

[11] Palacios, D.M., Bograd, S.J.: A census of Tehuantepec and Papagayo eddies in the northeastern tropical Pacific. Geophysical Research Letters **32**(23), 23606 (2005)

[12] Purkiani, K., Paul, A., Vink, A., Walter, M., Schulz, M., Haeckel, M.: Evidence of eddy-related deep ocean current variability in the North-East Tropical Pacific

Ocean induced by remote gap winds. Ocean Science **16**(6), 1443–1464 (2020)

[13] Chang, C.-H., Xie, S.-P., Schneider, N., Qiu, B., Small, J., Zhuang, W., Taguchi, B., Sasaki, H., Lin, X.: East Pacific ocean eddies and their relationship to subseasonal variability in Central American wind jets. Journal of Geophysical Research: Oceans **117**(C10), 10001 (2012)

[14] Chelton, D.B., Schlax, M.G., Samelson, R.M.: Global observations of nonlinear mesoscale eddies. Progress in Oceanography **91**(2), 167–216 (2011)

[15] Atlas, R., Hoffman, R.N., Ardizzone, J., Leidner, S.M., Jusem, J.C., Smith, D.K., Gombos, D.: A cross-calibrated, multi-platform ocean surface wind velocity product for meteorological and oceanographic applications. Bulletin of the American Meteorological Society **92**(2), 157–174 (2011) https://doi.org/10.1175/2010BAMS2946.1

[16] Mears, C.A., Lee, T., Ricciardulli, L., Wang, X., Wentz, F.J.: Improving the CCMP ocean surface wind vector dataset using new satellite observations and intercalibration. Remote Sensing **14**(22), 5719 (2022) https://doi.org/10.3390/rs14225719

[17] Le Vu, B., Stegner, A., Arsouze, T.: Angular momentum eddy detection and tracking algorithm (AMEDA) for multiscale eddy analysis. Journal of Atmospheric and Oceanic Technology **35**(4), 739–762 (2018) https://doi.org/10.1175/JTECH-D-17-0010.1

[18] Blumberg, A.F., Mellor, G.L.: A description of a three-dimensional coastal ocean circulation model. In: Heaps, N.S. (ed.) Three-Dimensional Coastal Ocean Models. Coastal and Estuarine Sciences, vol. 4, pp. 1–16. American Geophysical Union, Washington, D.C. (1987). https://doi.org/10.1029/CO004p0001

[19] GEBCO Compilation Group: GEBCO 2025 Grid. British Oceanographic Data Centre, NERC. Dataset de batimetría global grilla (2025). https://doi.org/10.5285/gebco-2025-grid . https://www.gebco.net/data_and_products/gridded_bathymetry_data/

[20] McCreary, J.P. Jr., Lee, H.S., Enfield, D.B.: The response of the coastal ocean to strong offshore winds: With application to circulations in the Gulfs of Tehuantepec and Papagayo. Journal of Marine Research **47**(1), 81–109 (1989)